Cell and tissue response to nanotextured Ti6Al4V and Zr implants using high-speed femtosecond laser-induced periodic surface structures

Article *in* Nanomedicine Nanotechnology Biology and Medicine · June 2019

DOI: 10.1016/j.nano.2019.102036

CITATIONS
8

READS
276

8 authors, including:

Iaroslav Gnilitskyi
Università degli Studi di Modena e Reggio Emilia
29 PUBLICATIONS **189** CITATIONS
SEE PROFILE

Pogorielov V Maksym
Sumy State University
65 PUBLICATIONS **237** CITATIONS
SEE PROFILE

Roman Viter
University of Latvia
99 PUBLICATIONS **1,239** CITATIONS
SEE PROFILE

Ana Maria Ferraria
University of Lisbon
165 PUBLICATIONS **1,642** CITATIONS
SEE PROFILE

Nanomedicine: Nanotechnology, Biology, and Medicine
21 (2019) 102036

nanomedjournal.com

Cell and tissue response to nanotextured Ti6Al4V and Zr implants using high-speed femtosecond laser-induced periodic surface structures

Iaroslav Gnilitskyi, PhD[a,b,c,*], Maksym Pogorielov, PhD[d,e], Roman Viter, PhD[f], Ana Maria Ferraria, PhD[g], Ana Patrícia Carapeto, PhD[g], Oleksandr Oleshko, PhD[d], Leonardo Orazi, PhD[a], Oleg Mishchenko, PhD[e]

[a]*University of Modena and Reggio Emilia, Reggio Emilia, Italy*
[b]*NoviNano Lab LLC, Lviv, Ukraine*
[c]*Department of Photonics, Lviv Polytechnic National University, Lviv, Ukraine*
[d]*Sumy State University, Sumy, Ukraine*
[e]*Osteoplant R&D, Debice, Poland*
[f]*Institute of Atomic Physics and Spectroscopy, University of Latvia, Riga, Latvia*
[g]*Centro de Química-Física Molecular and IN and IBB, Instituto Superior Técnico, Universidade de Lisboa, Lisbon, Portugal*

Revised 27 April 2019

Abstract

In this paper, the effect of femtosecond laser nanotexturing of surfaces of Ti6Al4V and Zr implants on their biological compatibility is presented and discussed. Highly regular and homogeneous nanostructures with sub-micrometer period were imprinted on implant surfaces. Surfaces were morphologically and chemically investigated by SEM and XPS. HDFa cell lines were used for toxicity and cell viability tests, and subcutaneous implantation was applied to characterize tissue response. HDFa proliferation and in vivo experiments evidenced the strong influence of the surface topography compared to the effect of the surface elemental composition (metal or alloy). The effect of protein adsorption from blood plasma on cell proliferation is also discussed.

Key words: Nanotexturing; Cell proliferation; Fluorescence; HR-LIPSS; Femtosecond laser

Excellent mechanical properties, chemical resistance and biocompatibility allow for the wide use of Ti and Zr, making those metals suitable for applications in orthopedics and dental surgery. However, around 7% of dental implants become damaged 10 years after surgery. Implant loss may occur due to surgical trauma, infection during either the implant placement or the healing process, and instability of the implant due to premature loading.[1] About 50% of implant failure are defined as late losses, which occur due to loss of bone support.[2,3] Despite appropriate mechanical properties for the fabrication of prostheses, some materials exhibit loss of integration with the human tissues.[4] Surface topography is a key factor for successful metal-tissue integration. The osteointegration process, that is the direct anchorage of an implant by the formation of bony tissues without the growth of fibrous tissues at the bone/implant interface,[5] starts directly after implantation from blood protein and growth factors adsorption on implant surface with further cell attachment and proliferation.[6] Bone progenitor cells like mesenchymal stem cells (MSCs) and lining osteoblast produce collagen with further mineralization and bone remodeling. In this paradigm, surface topography and wettability are key parameters in determining implant/tissue interaction and osteointegration.[7]

Although the integrity of the implant–bone tissue interface is essential, the interaction between the gingival/mucosal soft tissue and the implant must also be considered.[8] The oral mucosa provides protection to the periodontal tissue, including alveolar bone, against bacteria and other deleterious stimuli, but when breached by implant placement, the continuity of this barrier is disrupted.[9] Direct connection of metal implant with soft tissue is a critical issue during abutment connection in dental surgery. Pure connection and presence of gaps between abutment and surrounding soft tissue may lead to infection development and to implant failure.[10,11]

*Corresponding author.
E-mail address: jjyaroslav@gmail.com. (I. Gnilitskyi).

https://doi.org/10.1016/j.nano.2019.102036
1549-9634/

The implant surface should be modified to improve its biological response and to promote faster implant-tissue connection with greater efficiency. Namely, the roughness of the implants should enhance the attachment, proliferation, and differentiation of progenitor bone cells while the implant is in contact with the surrounding tissues to accelerate bone attachment.[12]

Various treatments have been developed to modify the implants surface, including machining/micromachining, sand-blasting, acid etching, electropolishing, anodic oxidation, and plasma spraying,[13] but it is still not clear which is the optimal topography for a better osteointegration. It was shown that the cells need cavities or grooves on the implant surface equivalent to or larger than their own size which is of ~30 μm.[14] In the case of a Ti surface roughened by sand-blasting with large grit, followed by acid etching, shallow spaces 20–30 μm in average diameter. Cells cultured on this surface occupied preferentially those cavities. Wennerberg et al. found by histology examination that optimal implant surface shown wavy structures with an average wavelength of 11.6 μm and with deviations in height by 1.4 μm.[15] From rabbit intermedullary implantation studies, it was found that lamellar bone and bone remodeling are highly favored by 200 μm pores created by laser compared to 10–25 μm ones.[16] Hulbert et al. also observed a similar relationship between osteons and growth on porous surface. Studies carried out on ceramic implants revealed that osteons require mini pores whose diameters range from 150 to 200 μm.[17] Also, Li et al. showed that bone growth on 140 μm pore size yielded the best results among all.[18] On the other hand, Linez-Bataillon found that smooth surfaces are more attractive for osteoblast MC3T3 cells and show significant better proliferation compared to sand-blasted implants.[19]

However, it was proven that scaffolds with nanoscale roughness have large surface areas to adsorb proteins, which present more binding sites to cell membrane receptors.[20] Lai et al. indicated that the nanostructured Ti coating enhances protein polymerization, osteoblast adhesion, or osteointegration,[21] whereas surfaces with rough textures increase the substrate/tissue interlocking and promote osteoblast differentiation. The mechanisms of cell detection and response to the implant surface nanofeatures are still unclear. For instance, Liwen Lin proposed that proteins may "sense" the surface topography at the nanoscale; therefore, materials with microscale textured surfaces may be "rough or hostile" to cells but "smooth and friendly" in presence of nanoscale textured surfaces.[22] Therefore, the contribution of nanostructures to implant-tissue integration still needs further study and characterization in order to figure out optimal method of dental and orthopedic implant surface treatment.

In spite of more than five decades of research in that field the formation of homogeneous LIPSS is still a challenge. Mechanisms of LIPSS formation by femtosecond laser pulses are not yet completely understood, but the common approach is based on the concept of interference between incident laser beam and laser-excited surface plasmon-polaritons supported by the presence of free electrons in metals,[23] the interference pattern during laser pulse consists of periodic maxima of total laser intensity at the metal-air interface imprinted by ablation into the metal surface. Those LIPSS on metal surfaces have found multiple applications in research on mechanics,[24] adhesion[25] and wettability.[26] However, transfer of the LIPSS technology to the real-world industrial and medical applications is limited by several technical challenges among which control of regularity, reproducibility of LIPSS over large surface areas, and low rate of LIPSS production are of major importance.

Although, Oktem et al. proposed a new method to generate LIPSS named Nonlinear Laser Lithography.[27] However, the physical model proposed by the authors was focused only on thin films and considered their oxidation; moreover, their approach is time consuming and presents low productivity rate. Those crucial issues still block the transfer of the femtosecond-LIPSS technology to industry and clinics.

The objective of the current research is to evaluate the biological response of in-vivo and in-vitro cell models attached to the surface of Zr and titanium alloy samples nanostructured by femtosecond laser pulses. The proposed nanostructuring method: Highly Regular LIPSS (HR-LIPSS) preserves the quality of nanostructures over a significant area of the nanotextured surface at an unprecedented treatment rate of about 15 mm^2/s,[24,28] HR-LIPSS combines micron-scale Low Spatial Frequency LIPSS (LSFL) with nano-scale roughness and is expected to be highly favorable for the osteointegration processes. The proposed approach that can guarantee high robustness and throughput rate is investigated in terms of cell viability and proliferation in order to evaluate the potential applications for surgery and dental implants.

Methods

Materials

Commercial grade-5 titanium alloy (Ti6Al4V) and zirconium (Zr, 99.7% purity) were purchased from Kurdumov Institute, NASU. The 10 mm diameter rods were cut in cylindrical slabs of 2 mm thickness. Subsequently, the slab surfaces were mechanically polished, resulting in surface roughness parameters (Table 2).

Laser setup and LIPSS surface texturing

The HR-LIPSS were imprinted on polished Ti6Al4V and Zr samples using a Light Conversion Pharos femtosecond Yb-doped solid state laser system. It delivers 213 fs pulses at central wavelength 1030 nm with a spectral width of 15 nm (FWHM). At pulse repetition rate of 600 kHz, the average output power is up to 20 W. The general scheme of the laser beamlines setup is shown in Figure 1.

The laser was then coupled to a galvanometer scanner system (ProSeries Cambridge Technology) equipped with an f-theta lens with 56 mm focal length resulting in a nominal laser spot diameter at $1/e^2$ intensity of 10.4 μm. This set up allows for scanning the metal surface at a linear speed of 3 m/s and an equivalent production rate of about 900 mm^2/min. The laser beam focused on the samples was scanned with bidirectional strategy in order to uniformly cover all the round samples. The parameter set is presented in Table 1.

An example of the HR-LIPSS treated surface on zirconium is shown in Figure 1. As visible at the glance, the surface appears

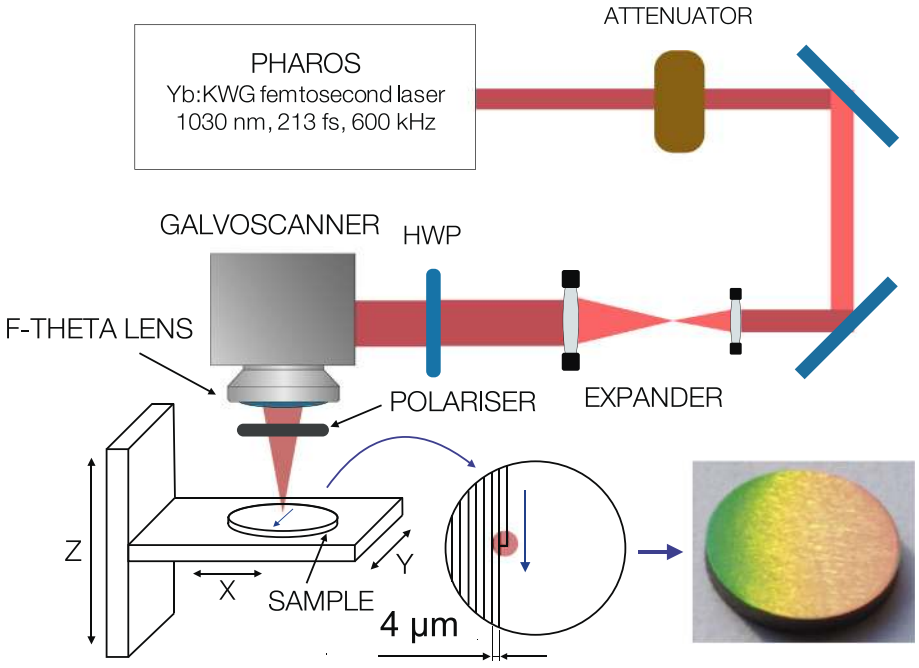

Figure 1. A laser setup for ultrafast laser writing of highly-regular periodic structures on metallic materials. HWP: half-wave plate.

Table 1
Laser parameters.

Material	Speed, mm/s	Step, µm	Pulse duration, fs	Repetition rate, kHz	Fluence, J/cm^2
Ti6Al4V	3000	4	213	600	0.6
Zr	3000	4	213	600	0.49

iridescent, a clear indication of the presence of sub-micrometer periodic structures. The iridescence is uniformly distributed indicating a good uniformity at large scale.

Surface characterization of samples treated by HR-LIPSS

The surface morphology was investigated by secondary electrons imaging and custom modes using a FEI Nova NanoSEM 450 with X-EDS Bruker QUANTAX-200. Cross sections were obtained and characterized by FEI Scios ultra-high-resolution analytical Dual-Beam system that reached the sub-surface layer using focused ion beam (FIB) technique. The surface morphology was imaged by AFM. The surface roughness was expressed in terms of arithmetic mean height (Ra) and maximum height (Rz) according to ISO 4287 standard and calculated from five different profiles. The chemical composition of the laser treated surfaces was investigated by X-ray photoelectron spectroscopy (XPS) with a XSAM800 KRATOS spectrometer operated in the fixed analyzer transmission (FAT) mode. Experimental conditions and data treatment details were described elsewhere.[29] The sensitivity factors Ti 2p: 2.098, Al 2p: 0.257, Zr 3d: 2.796, O 1 s: 0.736, and C 1 s: 0.318 were used for the calculation of the atomic concentrations.

Contact angle measurement

Contact angle (CA) measurements experiments were made using a video-based optical contact angle measuring instrument (OCA 15 EC, Data Physics, USA). The CA data was recorded for ultra-pure water, for at least 3 parallel samples.

Cell culturing

Samples with modified and non-modified surfaces (7 in each group) 10 mm in diameter were sterilized by 70% ethanol for 3 h at room temperature, washed in PBS twice and placed in 24-well plates. Dulbeccos Modified Eagle Medium (DMEM; Invitrogen, cat. no. 11960) supplemented with 10% Fetal Bovine Serum (FBS; Invitrogen), 2 mM L-glutamine (Invitrogen, cat. no. 25030), 0.1 mM 2-mercaptoethanol (Sigma, cat. no. M7522), 50 units/mL penicillin and 50 g/mL streptomycin (Invitrogen, cat. no. 15070) was added to each well, and incubated at 37 °C in a humidified environment with 5% CO_2. After 24 h, HDFa (Human Dermal Fibroblasts-Adult) were seeded at 10^4 cells per sample in 2 mL of DMEM. Samples with cells were incubated at 37 °C with 5% CO_2, and media was changed every 2 days during a 10-day culture period. All experiments were triplicates.

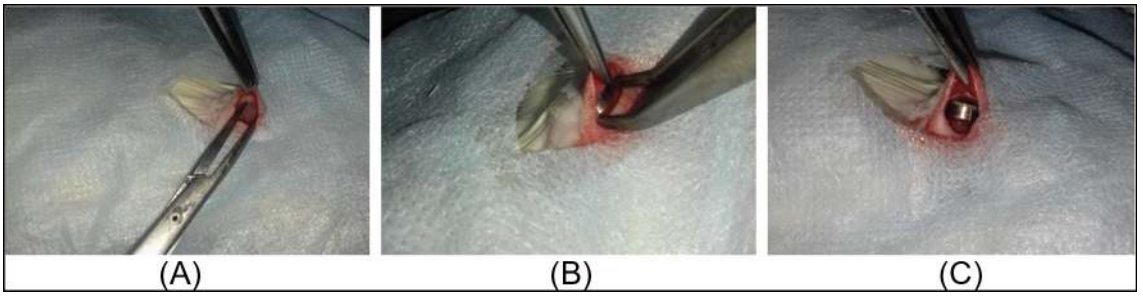

Figure 2. The in-vivo procedure for Ti6Al4V and Zr disks implantation. A – formation of subcutaneous pocket, B – Implantation procedure and C – Position of metal disk after implantation.

Cell viability

Alamar Blue (AB) assay was used to access cell viability on day 3, 7, 10 and 30 after seeding. Media was removed from each well and washed with PBS. One milliliter of Alamar Blue™ solution was added to each scaffold and incubated for 2 hours. Two aliquots of 200 μl of Alamar Blue™ solution was collected from each scaffold and read at a wavelength of 570 nm in a colorimetric plate reader to obtain baseline values of colorimetric absorbance.

Animal model

All animal procedures were approved by the Commission on Biomedical Ethics of Sumy State University (#14/06 on 14/06/2015). Thirty male laboratory rats, aged 8–9 months, were involved in the experiment. Animals were housed at 22 ± 2 °C on a 12 h light/dark cycle and received food and water ad libitum. Keeping of the animals and experiments were carried in accordance with the Directive 2010/63/EU of the European Parliament and of the Council of 22 September 2010 on the Protection of Animals Used for Scientific Purposes.

All animals were divided into two groups (15 in each) according to the type of alloy:

1. Group 1 (Control) –Ti alloy (sub-group 1) and Zr (sub-group 2) with smooth polished surface;
2. Group 2 – Ti alloy (sub-group 1) and Zr (sub-group 1) with modified surface;

The procedure of implantation included: after general anesthesia (ketamine, 10 mg per kg of animal weight) and peripheral vein catheterization, the back of animals was shaved in the intrascapular region. The surgical site was treated with C-4 solution (hydrogen peroxide and formic acid) and then a longitudinal incision was made. Subcutaneous tissues were separated from the skin above the left scapula and the implants were placed under the skin 1.0 cm from the incision (Figure 1, *A* and *B*). Before implantation all samples were sterilized in 70% ethanol during 30 min and washed in PBS twice. Finally, the wound was closed with simple interrupted sutures and aseptic dressing was applied (Figure 1, *C*).

After the operation, all the animals were kept in individual boxes to prevent additional trauma of the operation site. Animals were taken from experiment by overdose of narcosis (ketamine, 70 mg per 1 kg of animal weight) in 10 (15 rats) and 30 (15 animals) days after the implantation.

In vivo results assessment

Scanning electron microscopy

Samples were removed with care to prevent damage of the tissues that were covering implants (Figure 2). In case of capsule formation (2 control samples), they were cut and implants were removed. All the samples were put in 5% formaldehyde for 1 h, dehydrated in solutions of ethanol and dried in a vacuum set-up. To avoid surface charge accumulation in the soft tissue surface all the samples were covered with a thin (30–50 nm) layer of silver in the vacuum set-up VUP-5 M (SELMI). Scanning electron microscopy was performed by using the electron microscope REMMA102 (SELMI).

To analyze experimental results the following aspects were taken into account:

1. The presence of cells and fibers on the surface of the sample and their distribution;
2. Cells density per 1 mm^2;
3. Fibers size.

Statistics

One-way ANOVA with multiple comparisons was used to assess difference between groups using GraphPad Prism 8.0 software. Statistical significance was assumed at a confidence level of 95% ($P < 0.05$).

Results

Morphological analysis

The HR-LIPSS morphology on both pure Zr and Ti alloy was investigated by SEM. The images (Figure 3) reveal that nanostructures were successfully obtained on all the treated areas and they appear homogeneously distributed and regular. No bifurcations are present on both pure Zr and Ti alloy while some nanoparticles of recast materials are evident. The direction of the nanoripples is perpendicular to the laser polarization. The periods of nanostructures are 800 ± 42 nm for Zr and 820 ± 36 nm for Ti alloy. The roughness of the samples obtained from AFM profiles are given in Table 2.

On the basis of the FIB cross-sections reported in Figure 4a and Figure 5a for Zr and Ti6Al4V respectively, the thickness of ripples into the bulk is around 300–350 nm for both materials (Figures 4a(II) and 5a(II)). In accordance with SEM images of surface, regularity of periodic structures in cross-section is higher for Ti alloy than for Zr.

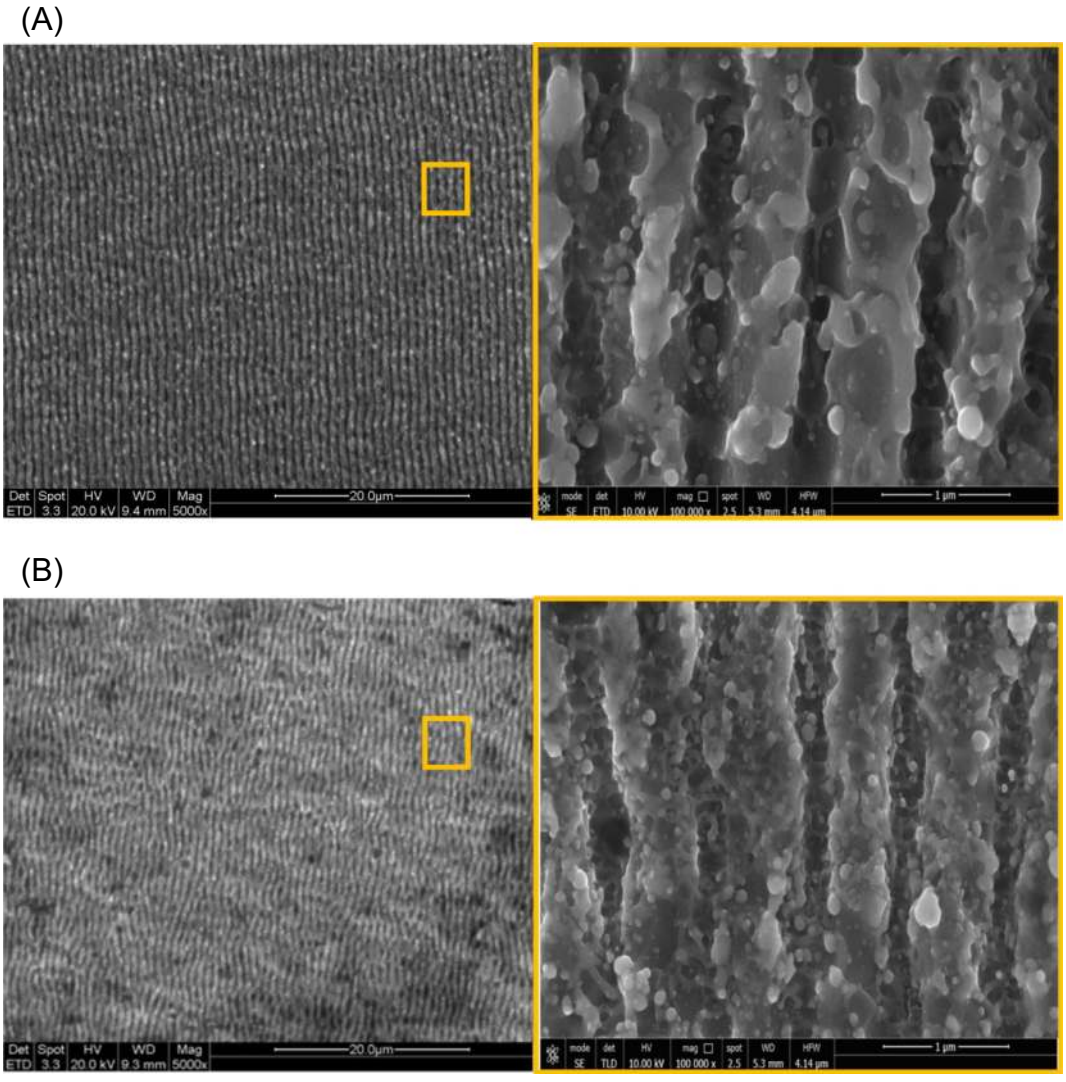

Figure 3. Modified surfaces of Ti-6Al-4 V (a) and Zr (b) by laser induced periodic surface structures (LIPSS).

Table 2
Roughness parameters.

Roughness parameters, μm	Polished Ti6Al4V	Polished Zr	LIPSS on Ti6Al4V	LIPSS on Zr
Ra	0.006	0.007	0.131	0.148
Rz	0.013	0.017	0.316	0.386

This is in good agreement with [28] and can be due to shorter period of plasmon-polariton wave on Ti surface in comparison with Zr.

As shown by the EDX maps both Ti alloy and Zr deep down the cross section of the sample, the oxygen is equally mixed with titanium Figure 4a(I) and zirconium Figure 5b(I). Above the periodic structures, on Ti6Al4V and Zr there is a visible thin film of oxygen, which is also confirmed by the XPS results.

Surface chemical analysis by XPS and wettability

The chemical composition of the treated and untreated surfaces of both Ti alloy and pure Zr were studied by XPS. Figure 6 shows the XPS regions of interest.

The surfaces are composed mainly by metal oxides and hydroxides, in particular TiO_2 and a small amount of Al^{3+} (Al_2O_3 and $Al(OH)_3$) in the Ti alloy and ZrO_2 in the Zr sample. Vanadium is on the tail of O 1 s region (Figure 6 (c)) and is barely detected: a not quantified peak, around ~517 eV, is assigned to V_2O_5 V $2p_{3/2}$ component.

In the Ti alloy, the main doublet in Ti 2p region (Figure 6 (a)) is assigned to TiO_2, with Ti $2p_{3/2}$ centred at 458.6 ± 0.1 eV; in the untreated surface, at lower binding energies (BE), Ti $2p_{3/2}$ peaks centred at 453.8 and 455.5 eV are assigned to Ti^0 and titanium suboxides at the interface metal/oxide, respectively; after treatment, Ti^0 is no longer detected and the relative amount of Ti suboxides decreases. Al 2p (Figure 6 (b)) is composed by 2

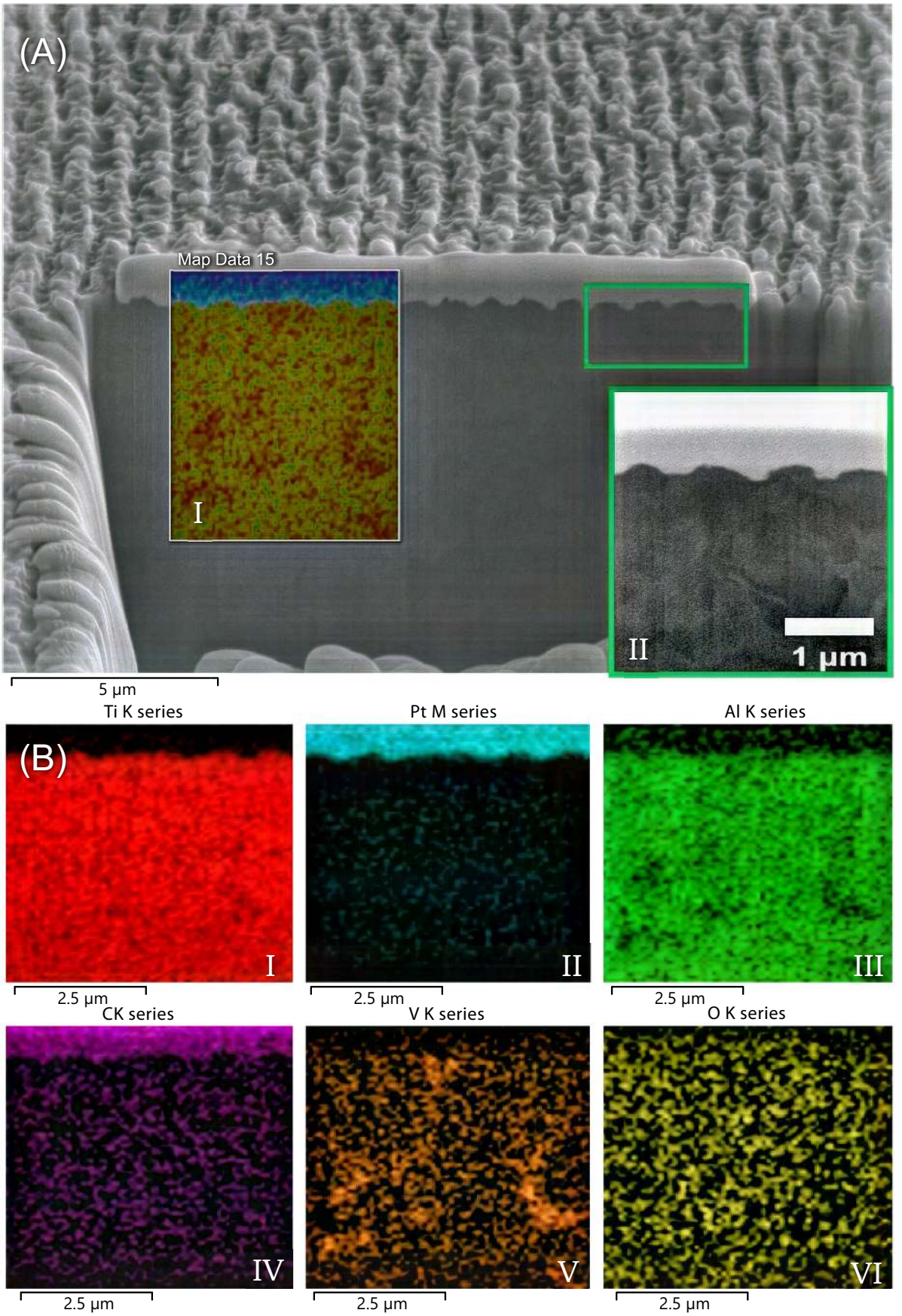

Figure 4. (a) SEM image of FIB cross-section with EDS (I) and FIB (II) insets of Ti alloy modified by HR-LIPSS. (b) EDS elements mapping of Ti6Al4V after HR-LIPSS treatment (I-VI).

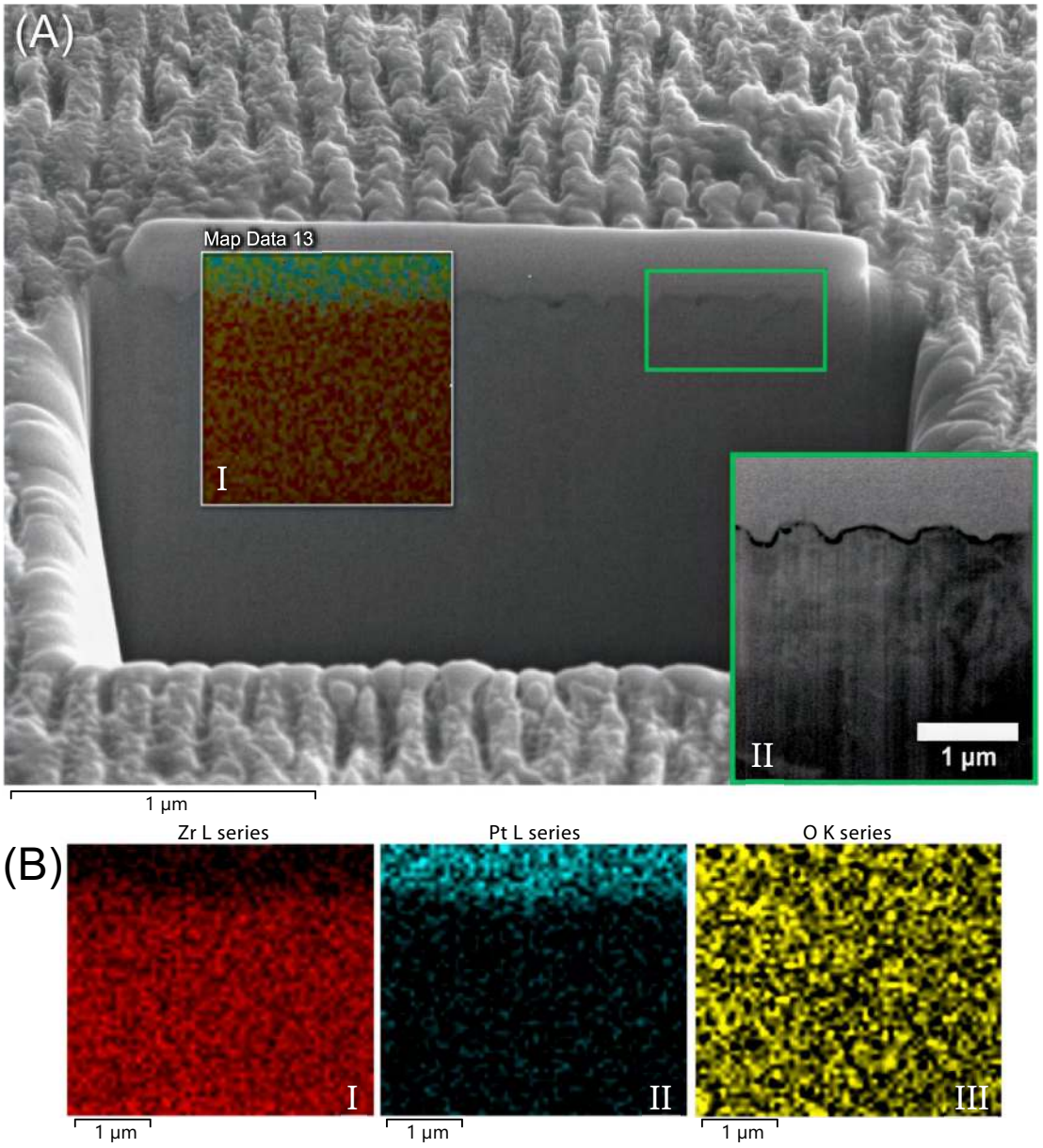

Figure 5. (a) SEM image of FIB cross-section with EDS (I) and FIB (II) insets of Zr modified by HR-LIPSS. (b) EDS elements mapping of Zr after HR-LIPSS treatment (I-III).

doublets, with the Al $2p_{3/2}$ peaks centred at 74.1 ± 0.2 eV and 76.2 ± 0.4 eV attributed, respectively, to Al_2O_3 and $Al(OH)_3$ or oxyhydroxides. C 1 s (Figure 6 (d)) reveals that some carbonaceous species are also present at the surface, in particular aliphatic carbon, carbon singly bound to oxygen and carboxylate groups, assigned to peaks in C 1 s centred at 285, 286.6 ± 0.1 and 288.8 ± 0.1 eV, respectively. In Figure 6 (e), O 1 s shows oxygen from metal oxides and hydroxides, centred respectively at 530.1 ± 0.1 and 531.8 ± 0.1 eV, and organic oxygen, as attested by the peak centred at 533.3 ± 0.2 eV attributed to oxygen singly bound to carbon and also by the peak assigned to the hydroxides which can also include oxygen doubly bound to carbon.

In pure zirconium, Zr 3d region of the untreated sample was fitted with 3 doublets (Figure 6 (f)), with the Zr $3d_{5/2}$ centred at 178.2 ± 0.2, 180.0 ± 0.3 and 182.3 ± 0.1 attributed, respectively, to Zr^0, that is hardly detected after treatment, to zirconium suboxides, most probably coming from the interface metal/surface oxides, which also decrease after treatment, and to ZrO_2 (the most abundant). Like in Ti6Al4V, the same types of carbonaceous species are detected at the surface of pure Zr (Figure 6 (g) and (h)).

Contact angle of non-treated polished surface was 80.66 ± 5.34^0 and 84.31 ± 6.2^0 respectively in Ti and Zr samples. After LIPSS treatment does not affect surface hydrophilicity with contact angle 85 ± 4^0 and 87 ± 5^0.

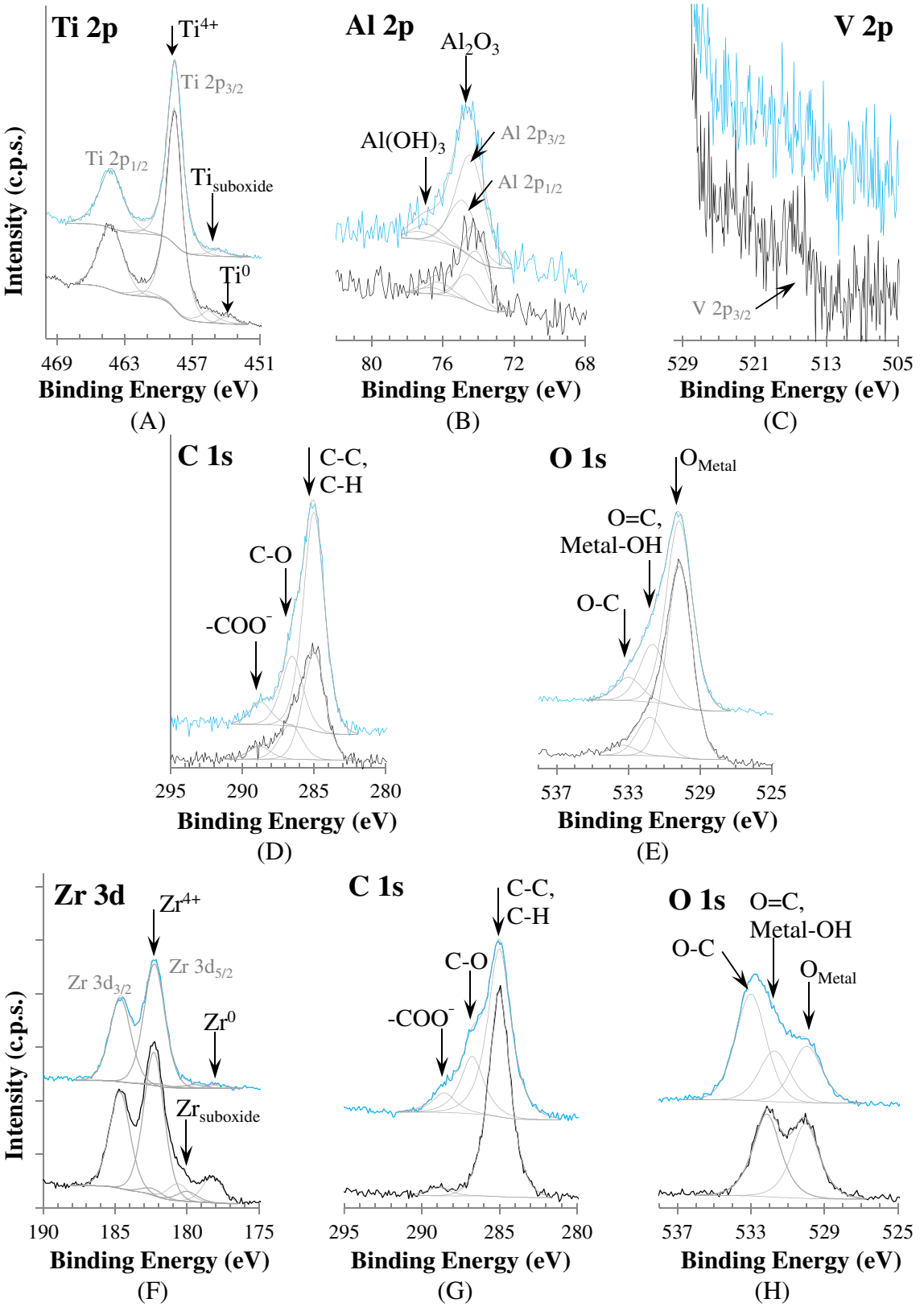

Figure 6. XPS regions of: Ti-6Al-4 V (a- e); and pure Zr (f-h). Top (blue spectrum): treated surface by laser; bottom (black spectrum): untreated surface.

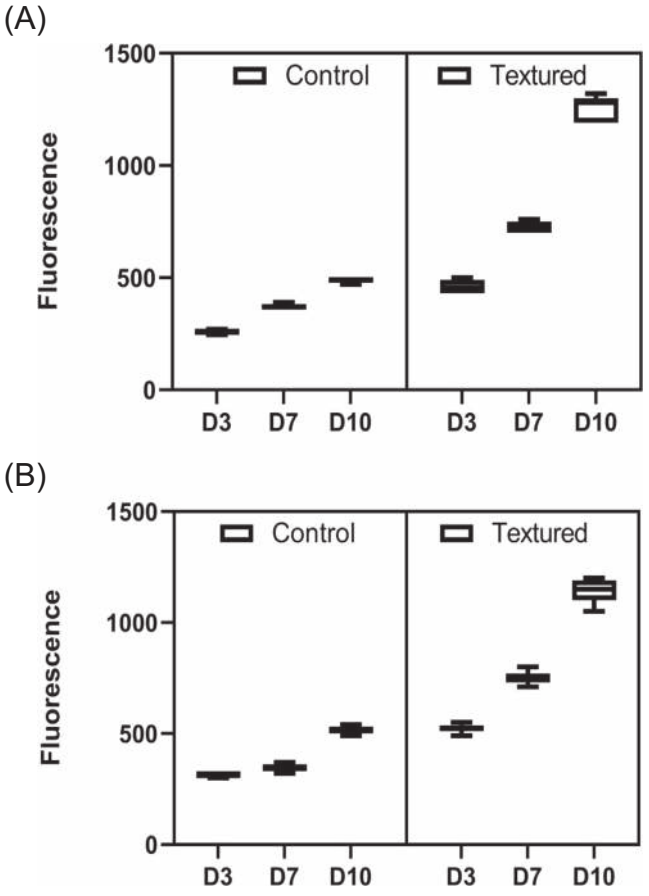

Figure 7. Cell viability of HDFa cells on Ti (a) and Zr (b) surface with different surface modification. Mean ± SD of the fluorescence of the media after the resazurin reduction assay, which is an indicator of metabolic activity. N = 3.

Cell culture

There was no significant difference between cells attachment and viability on Ti alloy and Zr. Fluorescent data indicate significant higher attachment (3rd day after cell seeding) on treated surface (459 ± 27 – for Ti and 523 ± 12 – for Zr) compare to polished implants (259 ± 9 and 315 ± 12). HDFa proliferated on control samples and fluorescence was significantly higher on day 7 and day 10 compared to the initial time point (day 3). Cell proliferation on treated surface shown 2 fold increasing in fluorescence on day 7 and day 10 compare the control ones (Figure 7).

Animal model

Both Ti alloy and Zr control implants (with smooth surfaces) were not covered with cells and fibers in 10 and 30 days after implantation (Figure 8, upper row). Single random fibers were observed, but probably they attached to samples during the samples removing procedure and have no bindings with metal surface. All implants were covered by thin capsule easily removed from them. Comparing to the control, all the modified samples were completely covered with connective fibers and cells in 10 days. Three types of cells were identified in current experiments erythrocytes, fibroblasts and leucocytes. Cells were on the fibers, that probably adsorbed to the metal surface in a first step after implantation. There is no difference in cells number and types between Ti alloy and Zr (Figure 8, middle row).

The number of erythrocytes and leucocytes are the same in both types of metal. The density of erythrocytes is 11.5 ± 2.9 per mm^2 and 13.3 ± 4.3 per mm^2 for the Ti alloy and for the Zr implants, respectively; the density of leucocytes is 3.6 ± 1.2 and 2.1 ± 0.5 per mm^2 for the same set of implants. However, the density of fibroblasts ranges from 7.4 ± 0.6 per mm^2 on Ti alloy and 8.8 ± 0.4 per mm^2 on Zr samples. Fibers covering the modified metallic implants were uniformly distributed on implant surface. Thin fibers with diameter less than 2 μm covered all surface and makes irregular bundles up to 20–30 μm in cross section dimension.

After the 30 days of implantation, treated metal implants were completely integrated with surrounding tissues and were hardly removed during operative procedures. Implant surface were completely covered with connective tissue-like structures with high amount of fibers. No specific cells were determined during SEM investigation.

Discussion

Surface topography and chemistry are essential parameters for the interaction between implant and surrounding tissues due to their influence on ion exchange, protein adsorption and cell adhesion and interaction. There are a lot of evidences that rough surfaces significantly increase tissue integration properties of different materials.[29,30] Modifications of metal surfaces are often employed as a means of controlling tissue-implant interactions and shortening the time of healing.

Nevertheless, the influence of roughness size and their topography are still under investigations. Current methods allow to makes surfaces with structures from nano- to microscale dimensions with different topography. Design of surfaces with high waviness and porosity in microscale dimensions allows bone ingrowth and induces strong bone interlocking, improving thereby the mechanical resistance and stability of the implant.[31] Most studies have shown that roughness sizes over 25 μm induce cells adhesion and proliferation, but pores larger than 200 μm in diameter induce slower bone formation than smaller pores.[32] Also, different responses to microscaled surface roughness can be observed in different cell types. Kunzler et al. have shown that osteoblasts prefers rougher surface whereas fibroblasts are favored by smoother areas.[33] Finally, the roughness or pore size from 25 to 150 μm are more appropriate for cell adhesion, proliferation and implant-tissue integration.

Many cell studies have shown the importance of the nanodomains in cell adhesion and proliferation.[34,35] Nanostructures on titania surfaces have also been shown to modulate the inflammatory response and to enhance osseointegration if kept in the appropriate ranges.[36,37] These studies suggested that nanoscaled domains have important roles in osseointegration irrespective of the underlying microstructure.[38,39] Small changes in roughness are accompanied by local changes in chemistry in a way that it is still speculative to unambiguously claim the role of

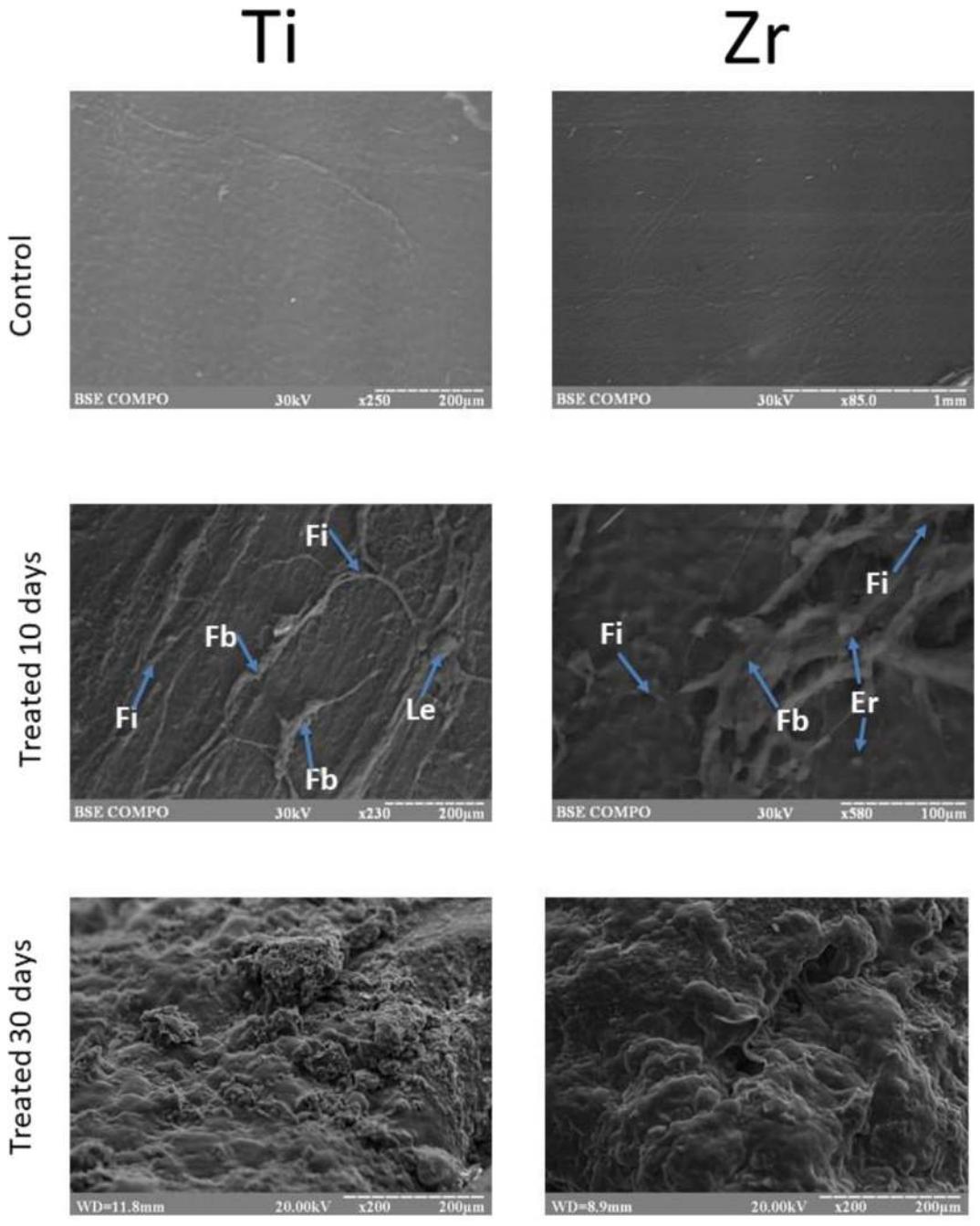

Figure 8. Surface of Ti alloy and Zr in untreated and treated after 10 and 30 days modes after the subcutaneous implantation. Surfaces of modified implants covered by the developed network of connective tissue fibers (Fi). Above the fibers we can observe erythrocytes (Er), leucocytes (Le) and fibroblasts (Fb). Please, change Ti to Ti6Al4V (in the Figure title).

structure alone in the biological environment.[40] Also, there are some evidences about changing of mechanical properties and corrosion resistance after nanoscale surface treatment. For example, titania nanotubes before and after annealing exhibit different corrosion properties and the titanate nanowire films, in fact, have inferior mechanical performance.[31]

Surface chemistry also plays an important role in protein adhesion. XPS investigation has shown the presence of hydroxides and carbonaceous species on the surface of the analyzed materials after HR-LIPSS treatment. Those species may promote the protein adsorption on the implant surface favoring both the platelet adhesion-activation and fibrin-binding accelerating implant healing and increasing the implant surface.[6]

Chemical patterns combined with structural features can influence on implant wettability, but current experiment did not show significant influence to contact angle for both Ti and Zr samples.

The experimental data presented in this work demonstrates a pronounced improvement of biological reaction of the nano-

structured implant surface as compared to polished non-structured ones. Probably, nano-topography allows faster and complete protein adsorption with next cells adhesion.[41,42] Roughly 2 time more cells on HR-LIPSS treated surface compared the non-treated ones on day 3 after cell seeding. Up to day 10 enhancement of cell proliferation in HR-LIPSS groups are observed and it is important to outline without any dependence with the metal, i.e. Ti alloy or Zr, was observed suggesting a predominant influence of surface topography. The proposed mechanism for cell attachment and proliferation starts with the early proteins adhesion on LIPSS-treated surface that provokes integrin-mediated cellular signaling cascades and stimulates cell proliferation.

In vivo experiments also showed that no cell adhesion occurred on a smooth surface in opposite to the laser-nanostructured ones. Different cell types, including fibroblast-like cells, migrate from blood and surrounded tissues on implant surface but cell adhesion we can see only in modified groups. Other in vivo studies have shown that regular smooth surface titanium surface have a presence of a dominant circular system of collagen fibers around the material.[43] Attached cells, predominantly fibroblasts, proliferate and produce fibers that integrate with implant surface. On day 30 after implantation we can observe complete integration of nano-structured surface with connective tissue and luck of tissue integration in smooth implants.

Conclusion

The use of femtosecond laser for the generation of HR-LIPSS on dental implants surfaces to improve cell adhesion and proliferation is reported. Results demonstrate a higher ratio of cells growth on laser-nanostructured surfaces compared to untreated ones. The surface characterization by XPS shows that the metal surfaces are highly oxidized (metal oxides and hydroxides). After laser treatment the metallic phase becomes less visible which may be due to an increase of the oxide/hydroxide layer and to some covering by an increased amount of oxidized carbonaceous species. The absence of dependence of cell proliferation on the type of metal (Ti alloy or Zr) and the strong dependence of cell proliferation on the topography and on the oxidation degree of the surface suggests a predominant role of the surface topography but also some influence of its composition on those biological processes. This fact opens great prospects for the HR-LIPSS method in the modification and improvement of the surface of dental and surgical implants.

Acknowledgments

The authors would like to thank Prof. A. M. Botelho do Rego (IST, University of Lisbon, Portugal) for the discussion of XPS results. Animal experiment was supported under the H2020-MSCA-RISE grant 777926 NanoSurf. AMF acknowledges FCT for financial support of Incentivo/CTM/LA0024/2014 and grant SFRH/BPD/108338/2015.

References

1. Pjetursson BE, Thoma D, Jung R, Zwahlen M, Zembic A. A systematic review of the survival and complication rates of implant-supported fixed dental prostheses (FDPs) after a mean observation period of at least 5 years. *Clin Oral Implants Res* 2010;**23**(Suppl 6):22-38.
2. Manor Y, Oubaid S, Mardinger O, Chaushu G, Nissan J. Characteristics of early versus late implant failure: a retrospective study. *J Oral Maxillofac Surg* 2009;**67**:2649-52.
3. Berglundh T, Persson L, Klinge B. A systematic review of the incidence of biological and technical complications in implant dentistry reported in prospective longitudinal studies of at least 5 years. *J Clin Periodontol* 2002;**29**:197-212 Suppl. 3.
4. Franz S, Rammelt S, Scharnweber D, Simon JC. Immune responses to implants – a review of the implications for the design of immunomodulatory biomaterials. *Biomaterials* 2011;**32**:6692-709.
5. Branemark P, et al. Immune responses to implants - a review of the implications for the design of immunomodulatory biomaterials. *Scand J Plast Reconstr Surg Suppl* 1977;**16**:1-132.
6. Mavrogenis AF, Dimitriou R, Parvizi J. G.C. Babis biology of implant osseointegration. *J Musculoskelet Neuronal Interact* 2009;**9**(2):61-71.
7. Xiao J, Zhou H, Zhao L, Sun Y, Guan S, Liu B. The effect of hierarchical micro/nanosurface titanium implant on osseointegration in ovariectomized sheep. *Osteoporos Int* 2011;**22**:1907-13.
8. Wong RL, Hiyari S, Yaghsezian A, Davar M, Casarin M, Lin YL, et al. Early intervention of peri-implantitis and periodontitis utilizing a mouse model. *J Periodontol* 2018 Feb 19, https://doi.org/10.1002/JPER.17-0541.
9. Wolfart S, Wolf K, Brunzel S, Wolfart M, Caliebe A, Kern M. Implant placement under existing removable dental prostheses and its effect on masticatory performance. *Clin Oral Investig* 2016 Dec;**20**(9):2447-55.
10. Javed F, Hussain HA, Romanos GE. Re-stability of dental implants following treatment of peri-implantitis. *Interv Med Appl Sci* 2013;**5**:116-21.
11. Canullo L, Penarrocha-Oltra D, Soldini C, et al. Microbiological assessment of the implant-abutment interface in different connections: Crosssectional study after 5 years of functional loading. *Clin Oral Implants Res* 2015;**26**:426-34.
12. Chen Wen-Cheng, Chen Ya-Shun, Ko Chia-Ling, Lin Yi, Kuo Tzu-Huang, Kuo Hsien-Nan. Interaction of progenitor bone cells with different surface modifications of titanium implant. *Materials Science and Engineering C* 2014;**37**:305-13.
13. Silverwood RK, Fairhurst PG, Sjöström T, Welsh F, Sun Y, Li G, et al. Analysis of Osteoclastogenesis/Osteoblastogenesis on Nanotopographical Titania. *SurfacesAdv Healthcare Mater* 2016;**5**:947-55.
14. Prevey PS, Loftus EF, Hornbach DJ. *J ASTM Int* 2006:3.
15. Wennerberg A, Hallgren C, Johansson C, Daneli S. *Clin Oral Implant Res* 1998;**9**:11-9.
16. Stangl R, Pries A, Loos B, Muller M, Erben RG. *J Biomed Mater Res* 2004;**69A**:444-53.
17. Hulbert SF, Young FA, Mathews RS, Klawitter JJ, Talbert CD, Stelling FH. *J Biomed Mater Res* 1970;**4**:433-56.
18. Li J, Liao H, Fartash B, Hermansson L, Johnsson. *Biomaterials* 1997;**18**:691-6.
19. Linez-Bataillon P, Monchau F, Bigerelle M, Hildebrand HF. In vitro MC3T3 osteoblast adhesion with respect to surface roughness of Ti6Al4V substrates. *Biomol Eng* 2002;**19**:133-41.
20. Yun H, Lin CJ, Li J, Wang JR, Chen HB. Low-temperature hydrothermal formation of a net-like structured TiO2 film and its performance of photogenerated cathode protection. *Appl Surf Sci* 2008;**255**:2113-7.
21. Lai YK, Lin CJ, Wang H, Huang JY, Zhuang HF, Sun L. Superhydrophilicesuperhydrophobic micropattern on TiO2 nanotube films by photocatalytic lithography. *Electrochem Commun* 2008;**10**:387-91.
22. Lin Liwen, Wang Hui, Ni Ming, Rui Yunfeng, Cheng Tian-Yuan, Cheng Cheng-Kung, et al. Changjian Lin enhanced osteointegration of medical titanium implant with surface modifications in micro/nanoscale structures. *Journal of Orthopaedic Translation* 2014;**2**:35-42.

23. Birnbaum M. Semiconductor surface damage produced by ruby lasers. *J Appl Phys* 1965;**36**:3688.
24. Gnilitskyi I, Pavlov F, Rotundo L, Orazi C Martini, Ömer Ilday F. *"Nonlinear Laser Lithography for Enhanced Tribological Properties", CLEO: AM2K.2*. Optical Society of America; 2015.
25. Rotella G, Orazi L, Alfano M, Candamano S, Gnilitskyi I. Innovative high-speed femtosecond laser nano-patterning for improved adhesive bonding of Ti6Al4V titanium alloy. *CIRP-JMST* 2017;**18**:101-6.
26. Cunha A, Paula Serro V, Oliveira A, Almeida R, Vilar M-C Durrieu. Wetting behaviour of femtosecond laser textured Ti-6Al-4V surfaces. *Appl Surf Sci* 2013;**265**:688-96.
27. Oktem I, Pavlov S, Ilday H, Kalaycioglu A, Rybak S, Yavas M Erdogan, et al. Nonlinear laser lithography for indefinitely large-area nanostructuring with femtosecond pulses. *Nature Photonics* 2013;**7**:897-901.
28. Derrien TJ-Y, Gnilitskyi I, Levy Y, Bugakova NM, Mocek T, Orazi L. High-speed, highly regular femtosecond laser printing of laser-induced periodic surface structures on metals: physical origin of the regularity. *Sci Rep* 2017;**7**:8485.
29. Cunha A, Elie A-M, Plawinski L, Serro AP, Botelho do Rego AM, Almeida A, et al. Femtosecond laser surface texturing of titanium as a method to reduce the adhesion of *Staphylococcus aureus* and biofilm formation. *Appl Surf Sci* 2016;**360B**(25):485-93, https://doi.org/10.1016/j.apsusc.2015.10.102.
30. Le Guéhennec L, Soueidan A, Layrolle P, Amouriq Y. Surface treatments of titanium dental implants for rapid osseointegration. *DentMater* 2007;**23**:844-54.
31. Wu Shuilin, Liu Xiangmei, Yeung Kelvin WK, Guo Huan, Li Penghui, Hu Tao, et al. Surface nano-architectures and their effects on the mechanical properties and corrosion behavior of Ti-based orthopedic implants. *Surface & Coatings Technology* 2013;**233**:13-26.
32. Stangl R, Pries A, Loos B, Müller M, Erben RG. Influence of pores created by laser superfinishing on osseointegration of titanium alloyimplants. *J Biomed Mater Res A* 2004;**69**:444-53.
33. Kunzler Tobias P, Drobek Tanja, Schuler Martin, Spencer Nicholas D. Systematic study of osteoblast and fibroblast response to roughness by means of surface-morphology gradients. *Biomaterials* 2007;**28**:2175-82.
34. Dalby MJ, McCloy D, Robertson M, Agheli H, Sutherland D, Affrossman S, et al. Osteoprogenitor response to semi-ordered andrandom nanotopographies. *Biomaterials* 2006;**27**:2980-7.
35. Lamers E, Walboomers XF, Domanski M, te Riet J, van Delft FC, Luttge R, et al. The influence of nanoscale grooved substrates on osteoblast behavior and extracel-lular matrix deposition. *Biomaterials* 2010;**31**:3307-16.
36. Domanski M, Luttge R, Lamers E, Walboomers XF, Winnubst L, Jansen JA, et al. Submicron-patterning of bulk titaniumby nanoimprint lithography and reactive ion etching. *Nanotechnology* 2012;**23** 065306/1–12.
37. Prodanov L, Lamers E, Domanski M, Luttge R, Jansen JA, Walboomers XF. The effect of nanometric surface texture onbone contact to titanium implants in rabbit tibia. *Biomaterials* 2013;**34**:2920-7.
38. Tran N, Webster TJ. Nanotechnology for bone materials. *WileyInterdiscip Rev Nanomed Nanobiotechnol* 2009;**1**:336-51.
39. Wennerberg A, Albrektsson T. On implant surfaces: a review ofcurrent knowledge and opinions. *Int J Oral Maxillofac Implants* 2010;**25**:63-74.
40. Tejero Ricardo, Anitua Eduardo, Orive Gorka. Toward the biomimetic implant surface: biopolymers ontitanium-based implants for bone regeneration. *Prog Polym Sci* 2014;**39**:1406-47.
41. Park JY, Gemmell CH, Davies JE. Platelet interactions with titanium: modulation of platelet activity by surface topography. *Biomaterials* 2001;**22**:2671-82.
42. Kikuchi L, Park JY, Victor C, Davies JE. Platelet interactions with calcium-phosphate-coated surfaces. *Biomaterials* 2005;**26**:5285-95.
43. Monica B-H, Raul AM, Enric J-S, Jose L-L. In fluence of surface modified dental implant abutments on connective tissue attachment: a systematic review. *Arch Oral Biol* 2017;**80**:185-92.